Naval Surface Warfare Center
Carderock Division
West Bethesda, MD 20817-5700

NSWCCD-50-TR–2000/053 **September 2000**

Hydromechanics Directorate

Technical Report

Numerical Simulation of Flow in Linear Cascade with Tip Clearance

by

Cheng-I Yang

NSWCCD-50-TR–2000/053 Numerical Simulation of Flow in Linear Cascade with tip Clearance

REPORT DOCUMENTATION PAGE

Form Approved
OMB No. 0704-0188

1. AGENCY USE ONLY *(Leave Blank)*

2. REPORT DATE
September 2000

3. REPORT TYPE AND DATES COVERED

4. TITLE AND SUBTITLE
Numerical Simulation of Flow in Linear Cascade with Tip Clearance

5. FUNDING NUMBERS
1-5080-172-54

6. AUTHOR(S)
Cheng-I Yang

7. PERFORMING ORGANIZATION NAME(S) AND ADDRESS(ES)
Propulsion and Fluid Systems Department, Code 5400
NSWC, Carderock Division
9500 MacArthur Blvd.
West Bethesda, MD 20817-5700

8. PERFORMING ORGANIZATION REPORT NUMBER
NSWCCD-50-TR-2000/053

9. SPONSORING / MONITORING AGENCY NAME(S) AND ADDRESS(ES)
Naval Sea Systems Command
93R
2531 Jefferson Davis Hwy
Arlington, VA 22242-5160

10. SPONSORING / MONITORING AGENCY REPORT NUMBER

11. SUPPLEMENTARY NOTES

12.a DISTRIBUTION / AVAILIBILITY STATEMENT
Approved for Public Release, Distribution Unlimited.

12.b DISTRIBUTION CODE

13. ABSTRACT *(Maximum 200 words)*

The evolution of the tip separation vortex, the tip leakage vortex and the passage vortex generated by flow over a low-speed linear compressor cascade with tip clearance was studied by solving the Navier-Stokes equations numerically. The discretization is based on flux-difference splitting, implicit high-resolution scheme. Up to a third-order accurate upwind differencing is achieved through a reconstruction of the solution from its cell averages. Balwin-Lomax turbulence model with blending function to account for the corner flow was used for the turbulence closure. The formation and the development of the vortices were simulated and were compared with experimental observation.

16. SUBJECT TERMS
Navier-Stokes Solver, Linear Cascade, Tip Leakage Vortex

15. NUMBER OF PAGES
22

16. PRICE CODE

17. SECURITY CLASSIFICATION OF REPORT	18. SECURITY CLASSIFICATION OF THIS PAGE	19. SECURITY CLASSIFICATION OF ABSTRACT	20. LIMITATION OF ABSTRACT
UNCLASSIFIED	UNCLASSIFIED	UNCLASSIFIED	SAME AS REPORT

(THIS PAGE INTENTIONALLY LEFT BLANK)

CONTENTS

FIGURES

NOMENCLATURE

c	chord length
l	span of the cascade blade
L_y	coordinate of tip vortex center from wall
L_z	coordinate of tip vortex center from suction surface
R	vortex core radius
Rn	Reynolds number $(V_{ref}\, c\,) / \nu$
s	pitch of the casade blade
V_{ref}	magnitude of the velocity at inlet midspan
V_x	velocity component in X direction
x	distance from the leading edge of the blade, in X direction
X,Y,Z	Cartesian coordinate system
ν	kinematic viscosity

ABBREVIATIONS

CPU	Central Process Unit
NACA	National Advisory Committee for Aeronautics
NAVSEA	Naval Sea Systems Command
NSWCCD	Naval Surface Warfare Center, Carderock Division
RANS	Reynolds Averaged Navier-Stokes
SGI	Silicon Graphics Incoperated
mm	millimeter
m/s	meter per second

(THIS PAGE INTENTIONALLY LEFT BLANK)

ABSTRACT

The evolution of the tip separation vortex, the tip leakage vortex and the passage vortex generated by flow over a low-speed linear compressor cascade with tip clearance was studied by solving the Navier-Stokes equations numerically. The discretization is based on flux-difference splitting, implicit high-resolution scheme. Up to a third-order accurate upwind differencing is achieved through a reconstruction of the solution from its cell averages. Balwin-Lomax turbulence model with blending function to account for the corner flow was used for the turbulence closure. The formation and the development of the vortices were simulated and were compared with experimental observation.

ADMINISTRATIVE INFORMATION

This work was sponsored by the Advanced Submarine R&D office (93R), Naval Sea Systems Command (NAVSEA) and administrated by the Advanced Propulsor Development Program Office (Code 508), Naval Surface Warfare Center, Carderock Division (NSWCCD). The work was conducted by the Hydromechanics Directorate, Propulsion and Fluid Systems Department (Code 5400), NSWCCD, under work unit number 1-5080-172-54.

INTRODUCTION

A structure of the flow in the blade row of a turbomachine is predominately three-dimensional. Vortices are generated near the blade surface and within the tip gap. The vortices of particular interest are the leading edge separation vortex, the leakage vortex and the passage vortex. Excessive activities of vortices may cause some detrimental effects, such as efficiency loss, noise generation, cavitation and blade erosion. Numerous experiments have been conducted to gain an understanding of the nature of the vortex flow [1,2,3,4,5,6,7,8]. Complementarily, numerical methods have been developed to facilitate predictions [2,9,10,11,12], so that an optimal design can be achieved.

The flow visualizations and measurements from the tip gap experiments conducted by Kang and Hirsch [3,4,5] clearly indicated that a multiple vortices structure existed around the blade tip. From the numerical simulation point of view, this experiment provides an ideal and challenging environment. Recent numerical simulations of the vortex related flows [2,9,13]

suggested that with a dense grid distribution and a high-order differencing technique detailed flow structure within the vortex core can be qualitatively simulated.

The purpose of the present study is to examine the feasibility of simulating the multiple vortices structure observed by Kang and Hirsch with a third-order accurate upwind finite-differencing high-resolution Reynolds-averaged Navier-Stokes (RANS) solver [14,15].

DESCRIPTION OF THE EXPERIMENT

The detailed description of the experimental facility, the setup and the offset of the blade section can be found in reference 3. Only a brief and computationally relevant outline is given here. The cascade consists of seven NACA 65-1810 blades having one free ends with flat tips. The aspect ratio is 1.0 with blade chord length of 200 mm. The pitch is 180 mm. The tip clearance is 2.0 percent of the chord length (4mm), with an uncertainty of ± 0.1mm for the seven tip gaps. The blade stagger angle is 10°. The blade inlet angle is 32.5° and the blade outlet angle is -12.5°. The mass averaged air inlet and exit angles, measured 40 % of chord length upstream and 25 % of chord length downstream are 29.3° and -2.5° (design values are 30° and -4.5°, respectively). The tests are conducted with the inlet flow velocity being kept constant at 23.7 m/s. The test Reynolds number Rn, based on the inlet velocity and the blade chord length is about 2.9×10^{5}. The free stream turbulence intensity is 3.4%.

A five-hole probe (the diameter of the sensitive part of the probe is 2.6 mm) is used to acquire the three-dimensional flow ahead of, within and behind the cascade. Surface static pressures (on both the wall and blade surfaces) are recorded by static pressure taps. The five-hole probe is calibrated in a jet. The accuracy of the measured velocity and total pressure are 1% of the inlet mid-span values where all the reference parameters are taken.

NUMERICAL SCHEME

The numerical solver is based on the three-dimensional incompressible Navier-Stokes equations expressed in the conservative law form. The equations are coupled with the continuity equation through the artificial compressibility. The diffusive terms are discretized with a central differencing scheme, and the convective terms are discretized with the Roe's flux-difference splitting scheme [16]. Third-order accuracy is achieved by reconstruction of the solution from its cell-averages [14,15]. The reconstruction is accomplished by linear interpolation of the characteristic variables in the computational domain. The non-TVD (Total Variation Diminishing) forms are used in order to avoid excessive diffusion in the vortex core region. Time

marching is performed with first-order accurate Euler backward time differencing. The Modified Baldwin-Lomax Model for three-dimensional flow formulated by Chima et al. [17] is used for turbulence closure.

GRID GENERATION

The Cartesian coordinates system is used to describe the cascade geometry. The X axis runs from upstream towards downstream, the Z axis points from the root of the blades towards the tip, and the Y axis is chosen along the pitchwise direction. The origin of the coordinates system is located on the blade leading edge at the root. The orientation of the blade is defined by its stagger angle (10^{o}).

The computational domain consists of two portions, one part is the passage bounded partially by the pressure side surface of one blade and the suction side surface of the adjacent blade in addition to the periodic boundaries, and the other part is the complementary tip gap region. The inlet plane is located three chord-lengths upstream of the blade's leading edge, and the outlet plane is located three chord-lengths downstream of the blade's trailing edge. Based on the H-H type topology, grid systems for blade passage and tip gap are generated with the Gridgen code (version 13.4). In the pitchwise direction, the grids are clustered near the blade surfaces. In the streamwise direction, the grids are clustered around the leading and the trailing edges. The grids are distributed according to the hyper-tangent rule. The first grid spacing off the solid surface is set to be 1×10^{-5}, in order to provide sufficient resolution for the turbulent viscous flow. At the given Reynolds number ($2.9\times10^{+5}$), the first turbulence coordinate y^{+} off the solid surface is about 1. Grid systems with three different sizes are generated to represent the passage zone. The sizes are 195×65×113 (in axial, pitchwise, and streamwise directions, respectively), 195×107×113, and 195×121×123. The grid size for the complementary tip gap zone is 111×33×33. For each of the grid systems, the total grid nodal points are 1.5 million, 2.5 million and 3.0 million, approximately. The increasing grid nodal point number is to support finer resolution of the vortex flow.

COMPUTATIONAL RESULTS

The results presented here were obtained from the computations based on the grid system of 3.0 million nodal points. Computations are carried out with 6 SGI Origin 2000 CPUs in parallel. Figure 1 shows the computed particle tracing of the vortices near the tip region. Figure 2 shows the schematic of the vortex structure, reconstructed through flow visualization from

experiment [4]. Comparison between Figures 1 and 2 indicates that formation of the observed tip separation vortex and the tip leakage vortex are successfully simulated. Figure 3 shows the ink trace visualization on the blade tip surface [4], and Fig. 4 shows the corresponding reconstructed schematic of the flow pattern [4]. Figure 5 shows the computed limited skin friction lines on the tip surface. Comparison among Figures 3-5, it can be concluded that the positions of the separation line (convergent line) and the reattachment line (divergent line) are predicted correctly. This is an indication that the essential flow pattern at tip gap is simulated correctly. Figure 6 shows the cross flow vectors and the particle traces in the tip gap located at 46% chord (x/c = 0.46). Flow enters from the pressure side (left) and exits to the suction side (right). Particle tracing shows that the flow separates and then re-attaches to the tip surface near the suction side, a separation bubble is formed. The bubble marks the passage of the tip separation vortex. At the leading edge of the bubble, two secondary separations can be seen. Along the solid surfaces, the boundary layers are developed. The shear layers with embedded vorticity are then discharged into the suction side of the blade. The rolling up of the entrapped vorticity constitutes the leakage vortex. The length of the reference vector at the up right of Figure 6 is equivalent to the magnitude of the inlet velocity at mid-span. Figures 7-10 show the cross flow velocity vectors and static pressure contours around the tip leakage vortex core on the various traverse planes at axial locations x/c=0.6, 0.8, 1.00 and 1.125, respectively. The length of the reference vector at the top of the figures represents the magnitude of the inlet velocity at midspan. The location of the center of the vortex, where the cross flow vector vanishes, nearly coincides with that of the minimum static pressure. In a previous grid refinement study conducted by Dacles-Mariani et al [2], it was shown that an average of 15-20 grid points (in each of the pitchwise and the spanwise directions) in the vortex core region are needed in order to adequately resolve the flow. Hsiao and Pauley drew similar conclusion in their study of the tip vortex flow generated by a marine propeller [9]. In the present study, the grid resolution at the core region, typically as indicated by the vectors in Fig. 8, is finer then the 20×20 (pitchwise and spanwise directions) distribution as recommended. Figure 11 shows the vorticity magnitude contours at various traverse planes at axial locations from x/c=0.20 to x/c=1.00 with an increment of 10% chord length. It shows that the initial vortex roll up occurs around x/c=0.20, and the vortex becomes fully developed at x/c=0.60. At this point the shape of the vortex becomes nearly axisymmetric. The vorticity magnitude attends its maximum values at x/c=0.8, and starts to decline further downstream. Ramaprian and Zhang [6] suggested that as the rolling-up process continues, several competing processes determine the peak vorticity magnitude within the vortex. The first of these is the continuous trapping, by the vortex, of the vorticity from the shear layer. This tends to increase the magnitude of the negative vorticity with distance. On the other hand, the second process, namely,

diffusion of the vorticity by viscosity and turbulence, tends to decrease the peak magnitude of the vorticity within the vortex. Figure 11 also indicates that near the trailing edge, just off the blade surface, a vortex similar to the secondary vortex as shown in Fig. 2, is developing. This secondary vortex can also be traced from the vector plot in Fig. 9. Figure 12 displays the perspective view of the tip vortices and the static pressure contours around their cores at various traverse planes from x/c=0.4 to x/c=1.0 with an increment of 10% chord length. The contours show that at the initial rolling-up stage the static pressure at the center of the core drops; after the vortex is fully developed, the static pressure starts to recover. This recovery begins about at x/c=0.80, the same location as the vorticity magnitude reaches its maximum values in as shown in Fig. 11. Figure 13 shows the cross flow streamlines at x/c=0.80. The left boundary is on the suction side surface of a blade and the right boundary is on the pressure side surface of the next blade. Two vortices are shown near the top. The one near the suction side surface is the tip leakage vortex, its shape is nearly axisymmetric. The other is the tip passage vortex. There are also two vortices near the root. One is the corner vortex and the other is the root passage vortex. Kang and Hirsch illustrated such vortices at root schematically as shown in Fig. 15 [3]. Detailed discussion of the formation of these vortices can be found in reference 3. Figure 14 shows the surface static pressure distribution on the blade tip and on the suction side. There is an indication of pressure trough in Fig. 14, near the tip on the suction side surface. The pressure trough is due to the influence of the low pressure in the center of the tip leakage vortex. Similar but less intensive pressure troughs can be found near the root, these are caused by the corner and root passage vortex as shown in Fig. 13. Such vortex induced pressure trough has been discussed, measured and computed previously [2,10,13]. Figure 16 shows the comparison of the measured and the computed static pressure at the center of the vortex core. The computation predicted lower values than were measured. Figure 17 shows the trajectory of the center of the vortex core obtained from both computation and measurement. The computed trajectory agrees with the measurement very well. Figure 18 shows the evolution of the vortex core radius obtained from both computation and measurement. As the leakage vortex exits the cascade passage (X/c>1.0), the shape of the vortex core becomes asymmetric. The radius of the core is an averaged value. The agreement between the computation and measurement in general is good. The measurement data shown in Fig.16 to Fig. 18 are extracted from reference 4.

Figure 19 shows the comparison of the computed and the measured static pressure distribution at the blade surface at mid-span. The agreement is good on both pressure and suction sides. Figure 20 shows the static pressure distribution near the blade tip (1.5% span from the tip). On the pressure side, the agreement between the prediction and measurement is good, however, there is a pronounced discrepancy in comparison on the suction side. The measurement data

shown in Figures 19 and 20 are extracted from reference 3. Figure 21 shows the blade to blade profiles of axial velocity at x/c=0.11. The agreement between the prediction and the measurement is good at both near tip and mid-span regions. The location x/c=0.11, at where the comparison is made, is upstream of the tip leakage vortex roll-up point. Similar velocity profiles are shown in Figs.22 and 23, for the axial locations at x/c=0.55 and x/c=0.99, respectively. At both locations, the calculations over predicted the magnitude of the velocity on suction side near the tip, where the flow is dominated by the passage of the tip leakage vortex. At mid-span, the calculated and the measured velocities agree well. The measurement data shown in Figures 21 to 23 are extracted from reference 10.

DISCUSSION AND CONCLUSION

The tip leakage vortex flow is a challenging subject for both experiment and computation. The experimental data from Kang and Kirsch [3,4,5] provided excellent information for a numerical simulation of a vortex flow. Detail flow separations around the tip were recorded and illustrated. The measurements were conducted with five-hole probe. Although the diameter of the sensitive part of the probe is small relative to the blade pitch (1.4%); however, it is not insignificant when compared with the diameter of the vortex core (10.8% at x/c=0.8). Limited information regarding to the experimental uncertainty can be found in reference 3.

For numerical simulation, three different grid sizes were used in order to support and resolve the large gradients of the static pressure and the velocity components within the small vortex core. The grid sizes are 1.5 million, 2.5 million and 3.0 million. The difference between the resulting static pressure at vortex center obtained from the calculations with 2.5 million and 3.0 million grid points is within 1%. In final calculation, grid distribution around the vortex is at least or better than the 20×20 (pitchwise and spanwise) distribution. The numerical differencing scheme representing the RANS equations is third-order accurate for the inviscid flux and second-order accurate for the viscous flux. Some common and more noticeable characteristics of the tip leakage vortex, such as rolling-up of the shear layer and the strengthening and weakening of the vorticity, are numerically simulated. The predicted trajectory of the center of the tip leakage vortex is closer to the blade surface than it was measured. The calculated radius of the vortex is somewhat smaller than it was measured. Comparing with the measurement, the calculation also predicted lower static pressure and higher velocity in the vortex core.

Overall, in comparison with the measurements, the numerical simulation over-predicted the strength of the tip leakage vortex. Yet, the developing, the transporting and the diffusing of the vortex were simulated reasonably well. A successful computation requires a high-order

accurate differencing scheme, a support of dense grid and a sophisticated turbulence model to provide correct diffusion at the vortex core.

ACKNOWLEDGEMENTS

The U.S. Navy Hydrodynamic/Hydroacoustics Technology Center at NSWCCD provided the high-speed parallel multi-processing computational resource required for present computation.

Figure 3: Ink-trace visualization on the blade tip surface.

(Kang and Kirsch [4])

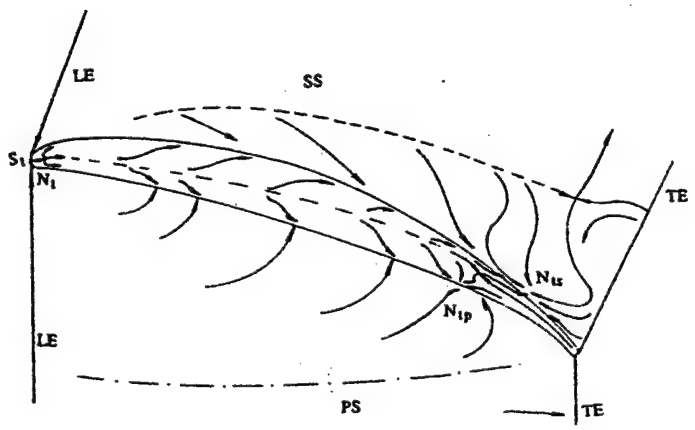

Figure 4: Schematic of the flow pattern on the blade tip.

(Kang and Kirsch [4])

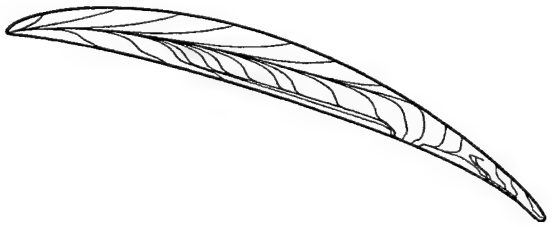

Figure 5: Computed limited skin friction lines on blade tip surface.

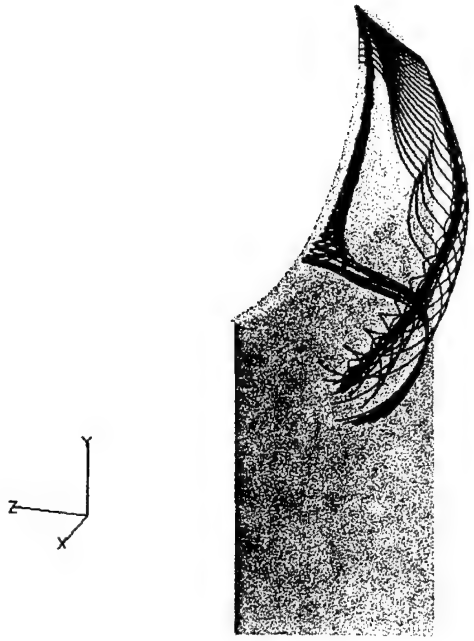

Figure 1: Particle tracing of vortices around tip gap.

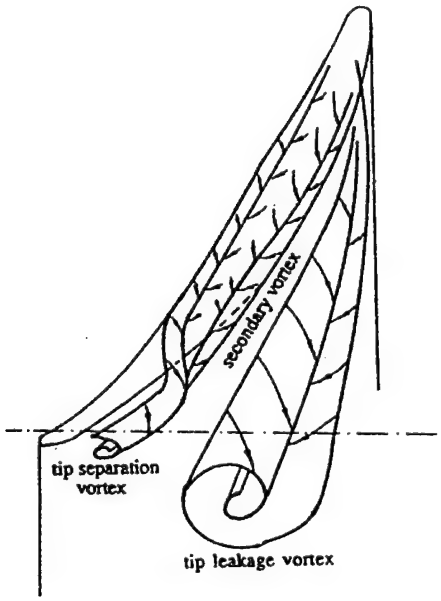

Figure 2: Schematic of the vortex structure around the tip gap.

(Kang and Hirsch [4])

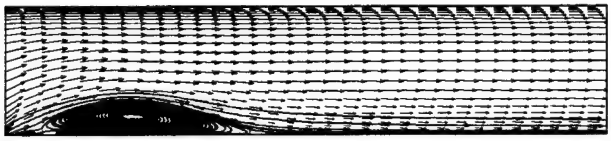

Figure 6: Cross flow vectors in tip gap at x/c = 0.46.

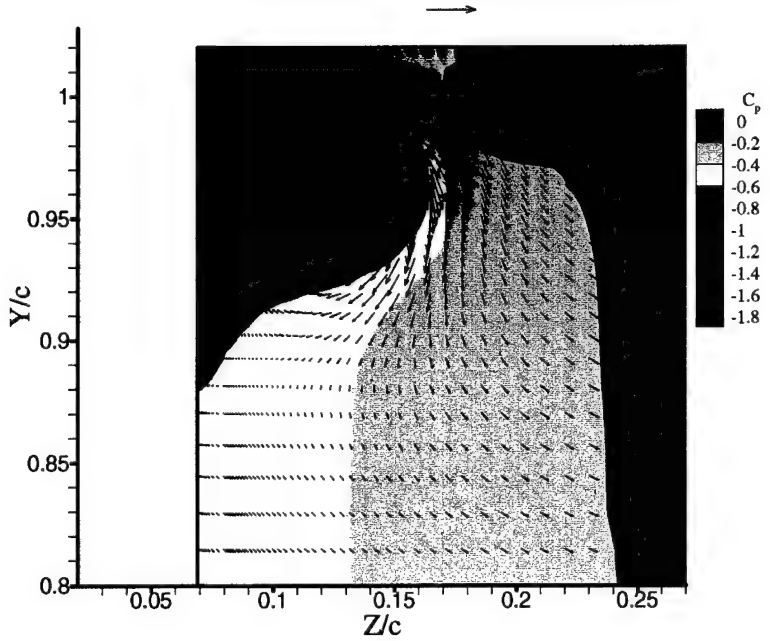

Figure 7: Cross flow vectors and static pressure contour around tip leakage vortex at x/c=0.60.

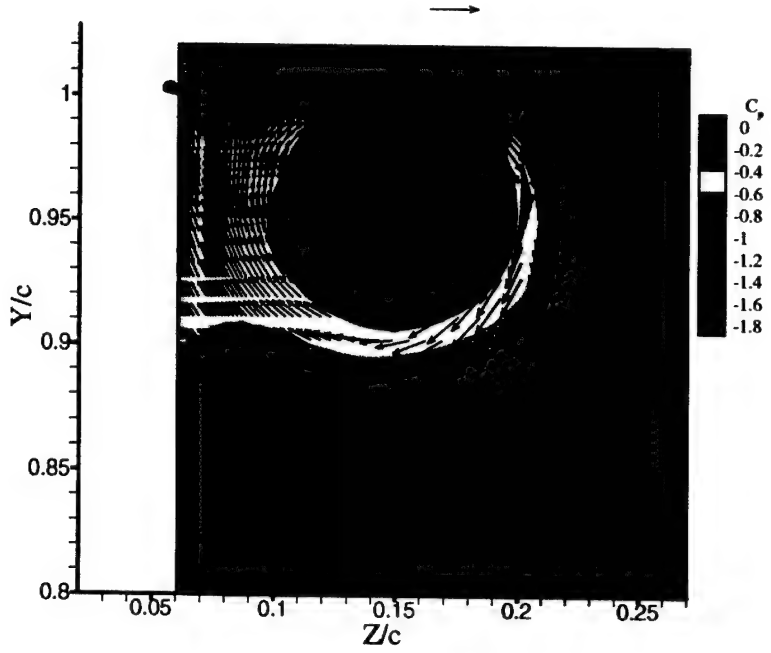

Figure 8: Cross flow vectors and static pressure contour around tip leakage vortex at x/c=0.80.

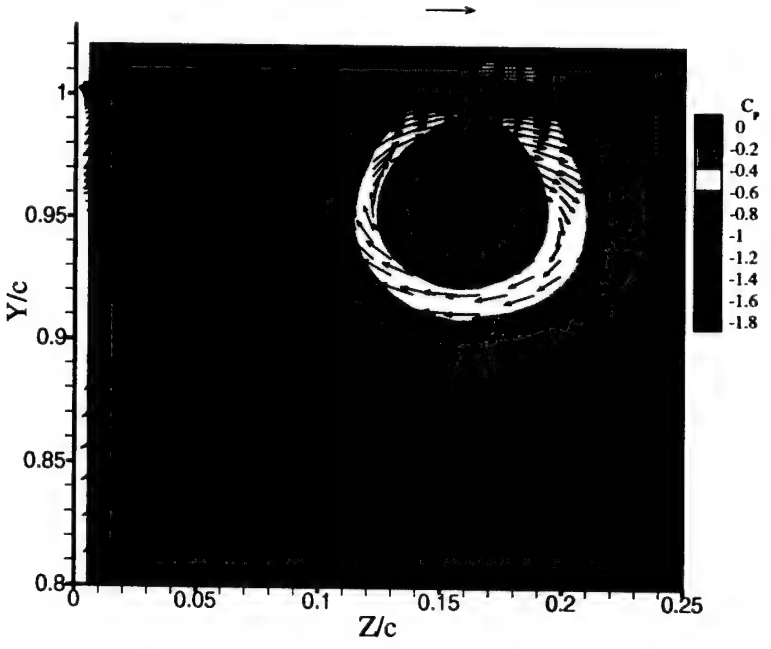

Figure 9: Cross flow vectors and static pressure contour around tip leakage vortex at x/c=1.00.

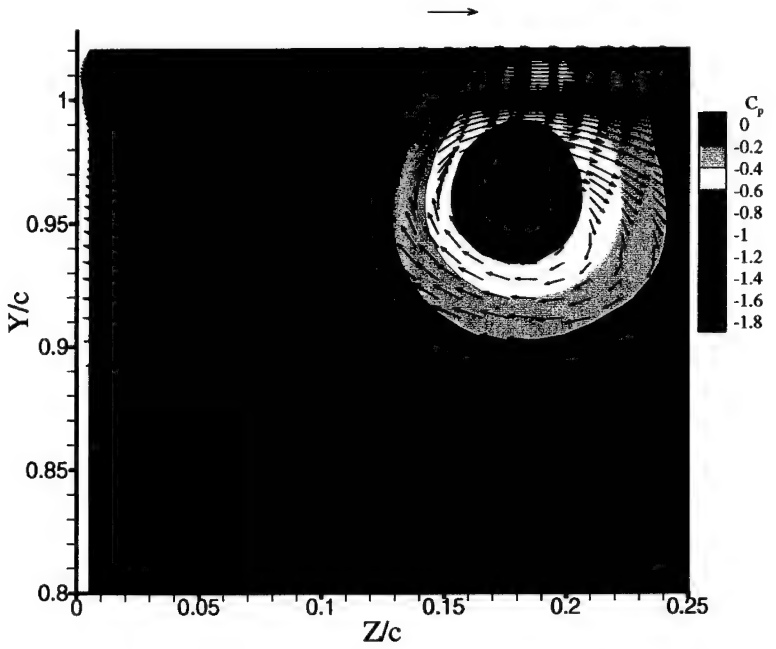

Figure 10: Cross flow vectors an static pressure contour around tip leakage vortex at x/c=1.125

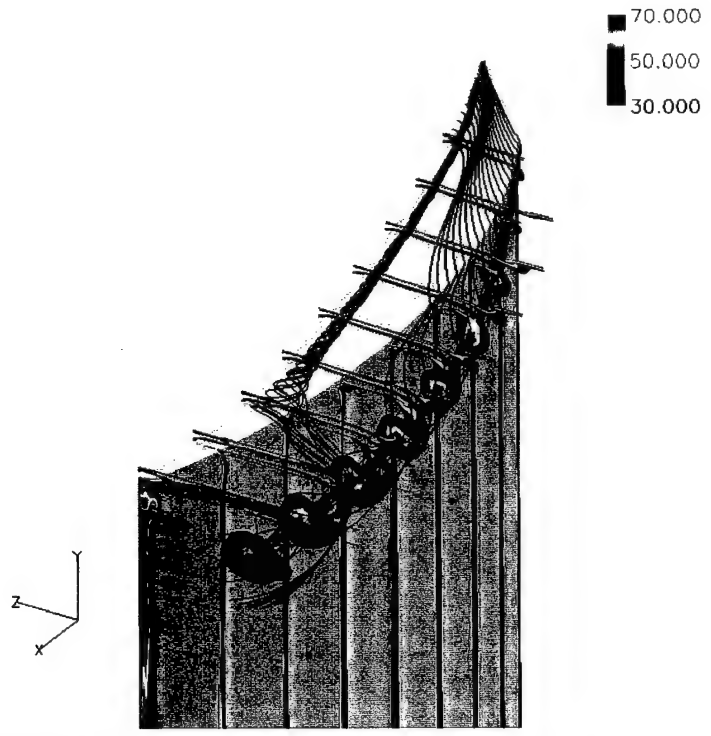

Figure 11: Particle tracing of the vortices around the tip gap with vorticity magnitude contours at various traverse planes.

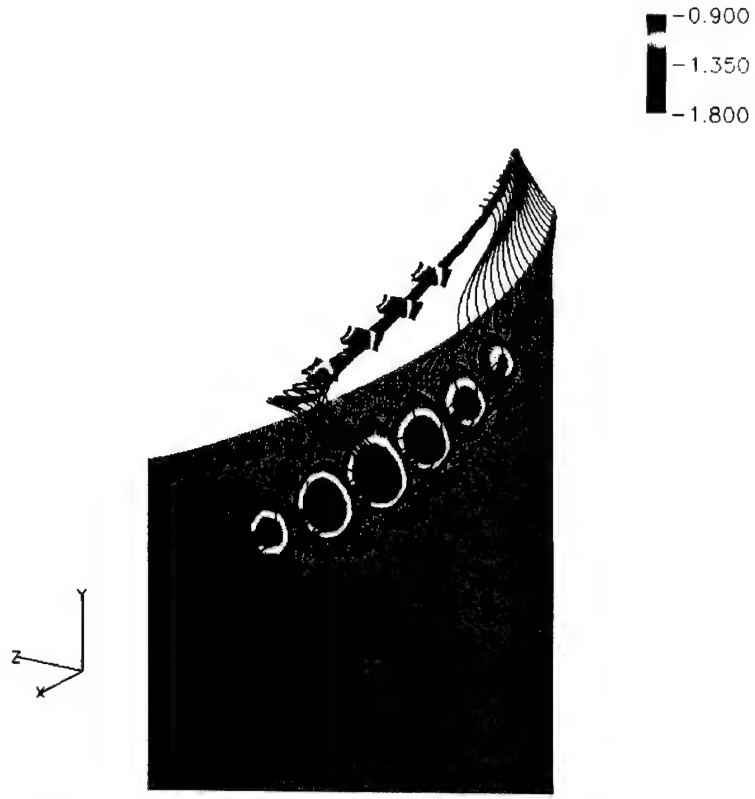

Figure 12: Particle tracing of the vortices around the tip gap with static pressure contours at various traverse planes.

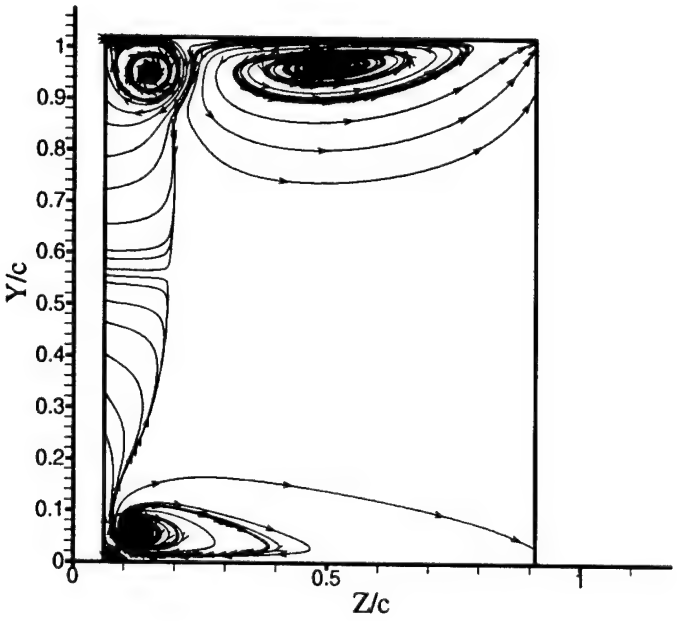

Figure 13: Cross flow streamlines at x/c=0.80.

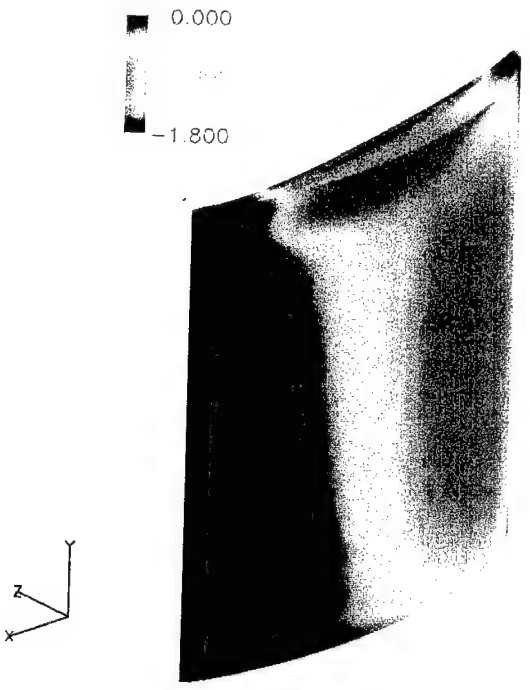

Figure 14: Surface static pressure contours at blade tip and suction side.

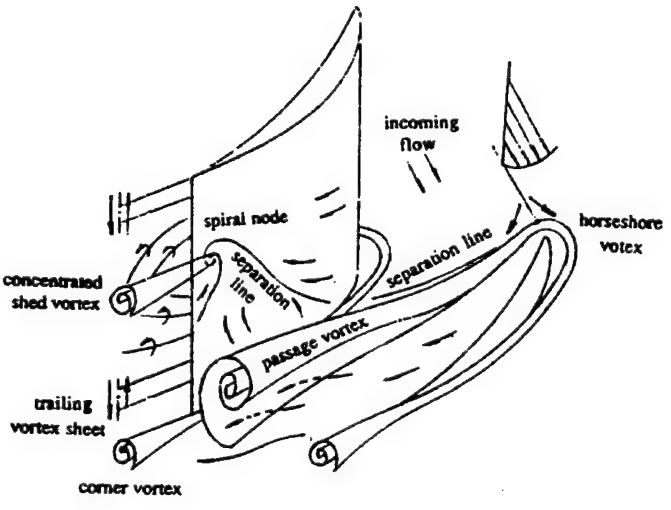

Figure 15: Secondary flow structure.

(Kang and Hirsch [3])

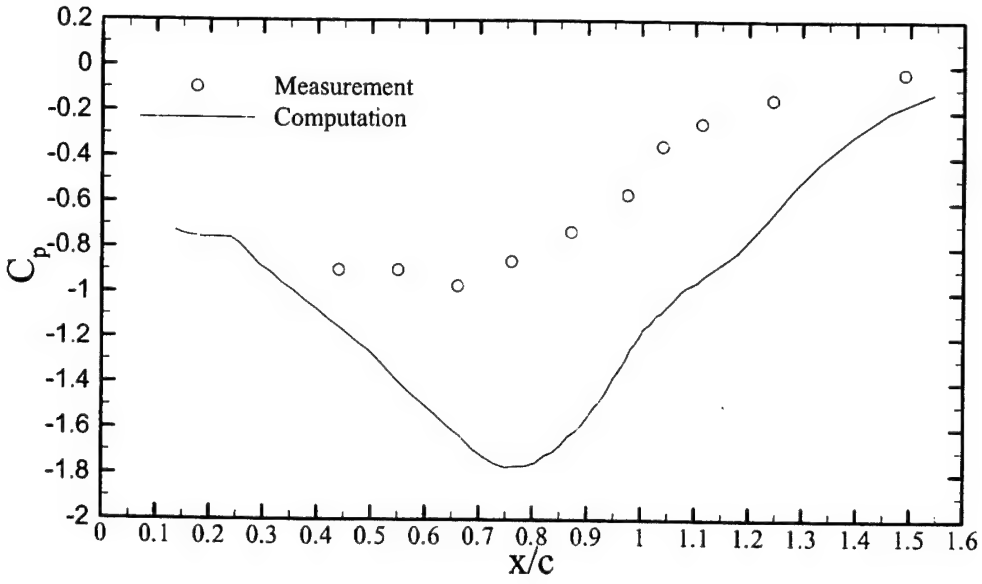

Figure 16: Static pressure at the center of the tip vortex core.

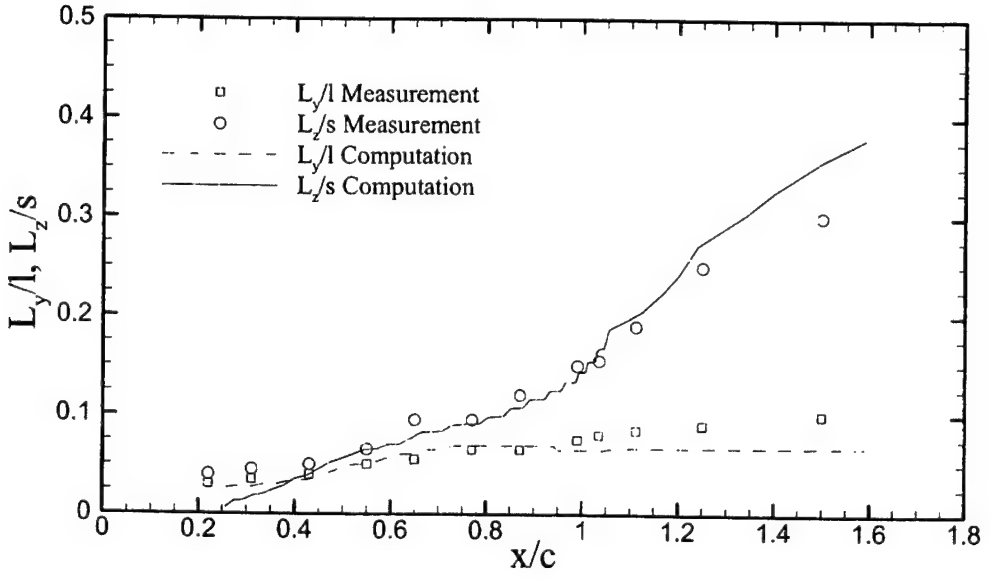

Figure 17: Evolution of the tip vortex center location in the mainstream direction.

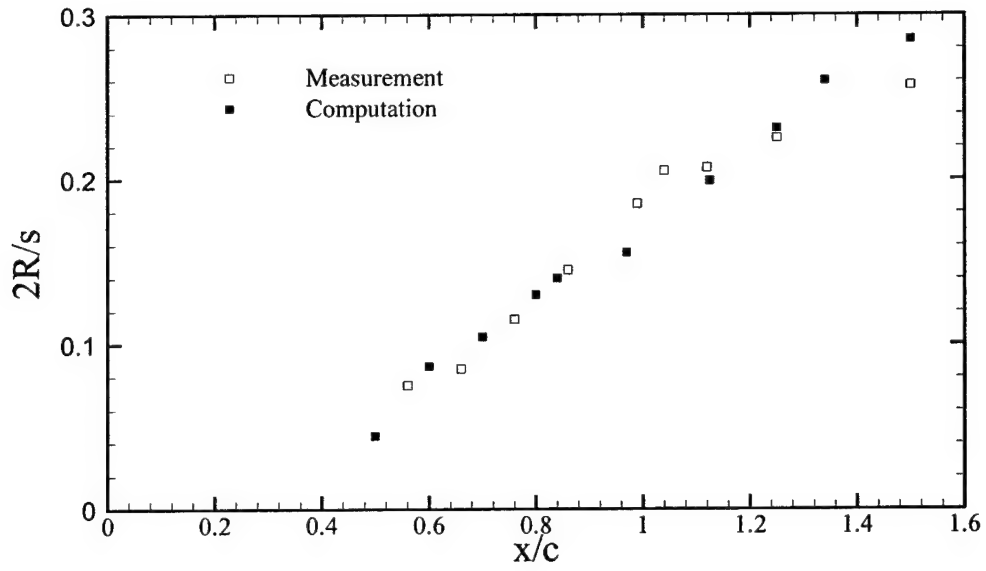

Figure 18: Evolution of tip vortex core radius in the mainstream direction.

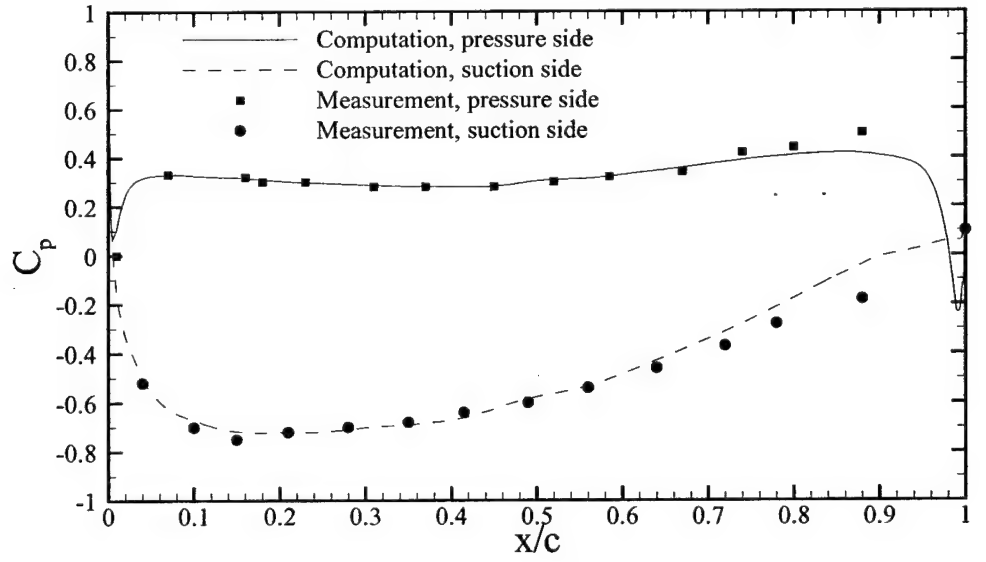

Figure 19: Static pressure distribution at blade surface at midspan.

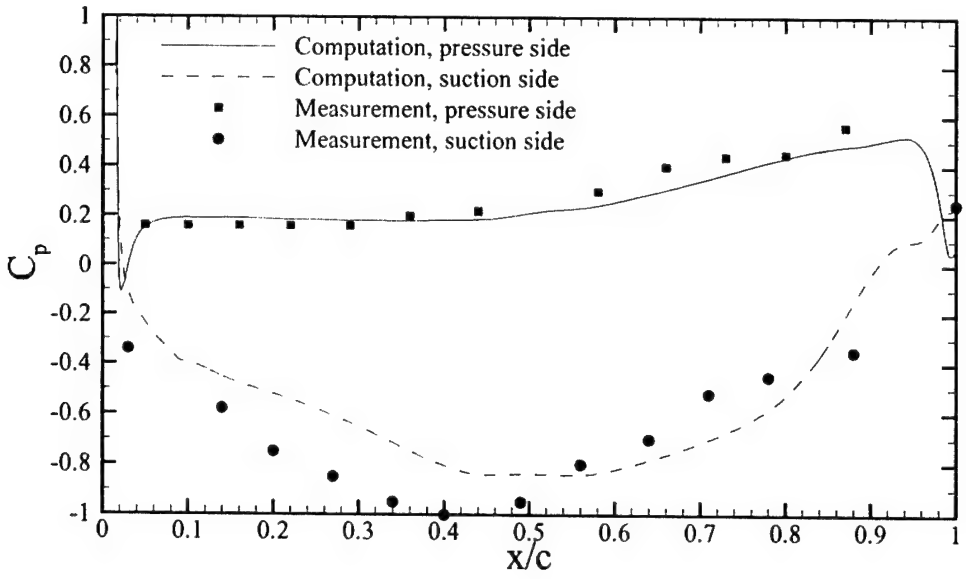

Figure 20: Static pressure distribution at blade surface at 1.5% span from the tip.

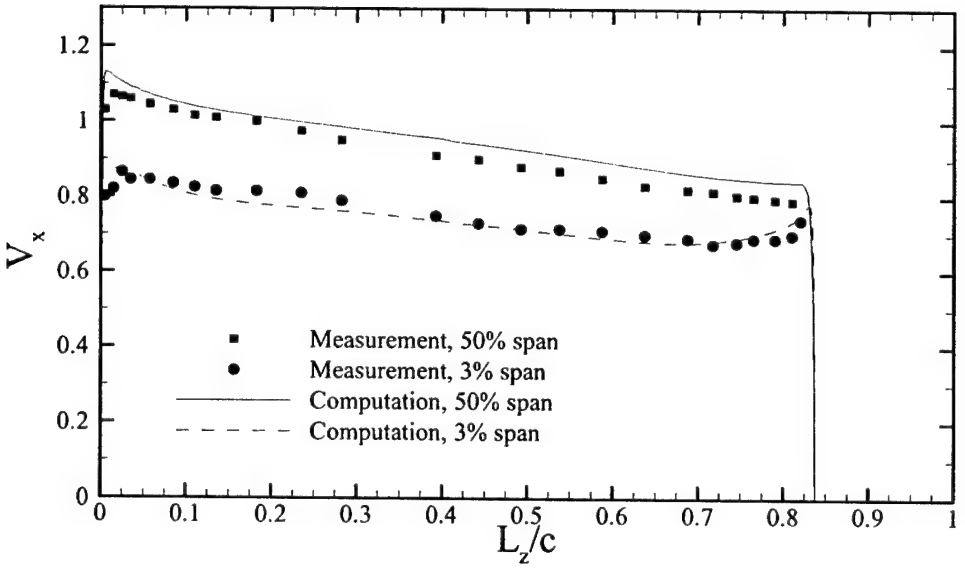

Figure 21: Blade to blade profiles of axial velocity at x/c=0.11.

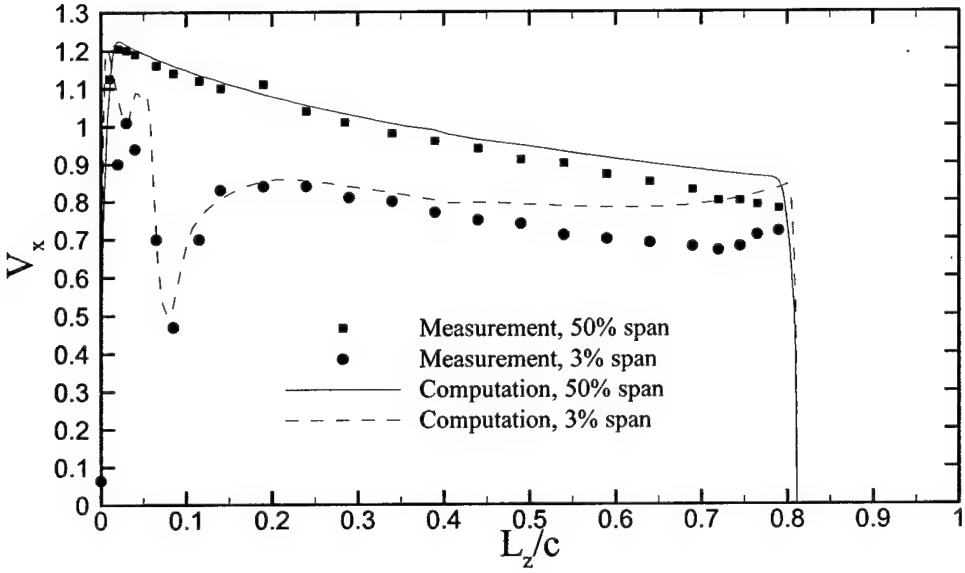

Figure 22: Blade to blade profiles of axial velocity at x/c=0.55.

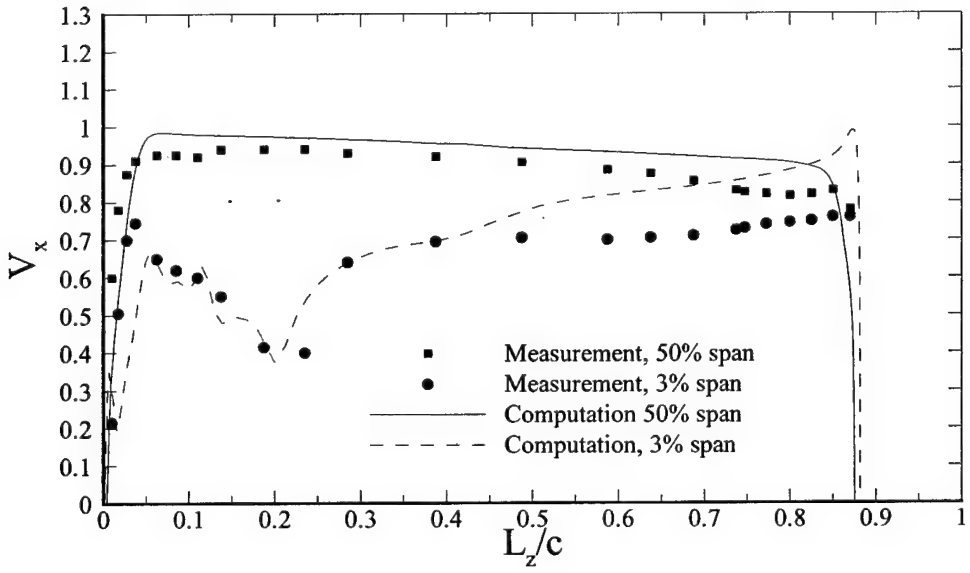

Figure 23: Blade to blade profiles of axial velocity at x/c=0.99.

(THIS PAGE INTENTIONALLY LEFT BLANK)

REFERENCES

1. Chesnakas, C.,J., and Jessup, S.D., "Propeller Tip-Vortex Measurements Using 3-Component LDV," *22nd Symp. on Naval Hydrodynamics*, Washington DC, (Aug. 1998).

2. Dacles-Mariani, J., Zilliac, G.G., Chow, J.S., and Bradshaw, P., "Numerical / Experimental Study of a Wingtip Vortex in the Near Field," *AIAA Journal*, Vol. 33, No. 9, pp.1561-1568 (1995).

3. Kang, S., and Hirsch, Ch., " Three Dimensional Flow in a Linear Compressor Cascade at Design Conditions," *ASME* Paper No. 91-GT-114, (1991).

4. Kang, S., and Hirsch, Ch., "Experimental Study on the Three Dimensional Flow within a Compressor Cascade with Tip Clearance: Part I – Velocity and Pressure Field," *ASME Journal of Turbomachinery*, Vol. 115, pp.435-443, (1993)

5. Kang, S., and Hirsch, Ch., "Experimental Study on the Three Dimensional Flow within a Compressor Cascade with Tip Clearance: Part I – Velocity and Pressure Field," *ASME Journal of Turbomachinery*, Vol. 115, pp.435-443, (1993)

6. Ramaprian, B,R., and Zheng, Y., "Measurements in Rollup Region of the Tip Vortex from a Rectangular Wing," *AIAA Journal*, Vol. 35, No. 12, pp.1837-1843, (1997).

7. Ramaprian, B.R., and Zheng, Y., "Near Field of the Tip Vortex Behind an Oscillating Rectangular Wing," *AIAA Journal*, Vol. 36, No. 7, pp1263-1269, (1998).

8. Shekarriz, A., Fu, T.C., Katz, J., and Huang, T.T., "Near-Field Behavior of a Tip Vortex," *AIAA Journal*, Vol. 31, No. 1, pp.145-152, (1993).

9. Hsiao, C-T., and Pauley, L.L., "Numerical Computation of Tip Vortex Flow Generated by a Marine Propeller," *ASME Journal of Fluid Engineering*, Vol. 121, pp. 638-645, (1999).

10. Kang, S., Hirsch, Ch., "Numerical Simulation of Three-Dimensional Viscous Flow in a Linear Compressor Cascade with Tip Clearance," *ASME Journal of Turbomachinery*, Vol. 118, pp.492-504, (1996).

11. Lee, Y-T, Feng, J., Merkle, C., and Tse, M., "Effects of tip-Clearance Flows," *21st Symposium on Naval Hydrodynamics,* National Academy of Science Press, Washington D.C., pp. 959-932, (1997).

12. Liu, J-S., and Bozzola, R., " Three-Dimensional Navier-Stokes Analysis of Tip Clearance Flow in Linear Turbine Cascades," *AIAA Journal*, Vol. 31, No. 11, pp. 2068-2074 (1993).

13. Hsiao, C-T., and Pauley, L.L., "Numerical Study of the Steady-State Tip Vortex Flow Over a Finite-Span Hydrofoil," *ASME Journal of Fluid Engineering*, Vol. 120, pp, 345-353, (1998).

14. Hartwich, P-M., and Hsu, C-H., "High-Resolution Upwind Schemes for the Three-Dimensional Incompressible Navier-Stokes Equations," *AIAA Journal* Vol. 26, No. 11, pp.1321-1328, (1988).

15. Yang, C-I., "A Simulation of Viscous Incompressible Flow through a Multiple-Blade-Row Turbomachinery with a High-Resolution Upwind Finite-differencing Scheme," *ASME, Numerical Simulations in Turbomachinery*, FED-Vol.227, pp. 11-18, (1995).

16. Roe. P.L., "Approximate Riemann Solver, Parameter Vectors, and Difference Schemes," *Journal of Computational Physics*, Vol.43, No.2, pp. 357-372, (1981).

17. Chima, R.V., Giel, P.W., and Boyle, R.J., "An Algebrac Turbulence Model for Three-Dimensional Viscous Flows," *31st Aerospace Sciences Meeting & Exhibit*, January 11-14, AIAA 93-0083, (1993).

INITIAL DISTRIBUTION

Code	Name
NAVSEA	
93R	D.Dahmar

CENTER DISTRIBUTION

Code	Name
508	J. Brown
54	J. Gorski
54	C-I Yang
54	B. Chen
54	S. Neely
54	S. Jessup

(THIS PAGE INTENTIONALLY LEFT BLANK)